Computational Model of Radiofrequency Ablation of Cardiac Tissues Incorporating Thermo-Electro-Mechanical Interactions

Singh S. and Melnik R.

Proceedings of the ASME 2020 International Mechanical Engineering Congress and Exposition (ASME IMECE-2020), Paper No: IMECE2020-23367, 8 pages. November 16 - 19, 2020, Portland, OR, USA. The American Society of Mechanical Engineers.

DRAFT

Proceedings of the ASME 2020
International Mechanical Engineering Congress and Exposition
IMECE2020
November 16-19, 2020, Portland, OR, USA

IMECE2020-23367

COMPUTATIONAL MODEL OF RADIOFREQUENCY ABLATION OF CARDIAC TISSUES INCORPORATING THERMO-ELECTRO-MECHANICAL INTERACTIONS

Sundeep Singh[1]
MS2Discovery Interdisciplinary Research Institute,
Wilfrid Laurier University,
75 University Avenue West,
Waterloo, Ontario, N2L 3C5, Canada

Roderick Melnik
MS2Discovery Interdisciplinary Research Institute,
Wilfrid Laurier University, Waterloo, Canada;
BCAM - Basque Center for Applied Mathematics,
Alameda de Mazarredo 14, E-48009 Bilbao, Spain

ABSTRACT

The application of radiofrequency ablation (RFA) has been widely explored in treating various types of cardiac arrhythmias. Computational modelling provides a safe and viable alternative to ex vivo and in vivo experimental studies for quantifying the effects of different variables efficiently and reliably, apart from providing a priori estimates of the ablation volume attained during cardiac ablation procedures. In this contribution, we report a fully coupled thermo-electro-mechanical model for a more accurate prediction of the treatment outcomes during the radiofrequency cardiac ablation. A numerical model comprising of cardiac tissue and the cardiac chamber has been developed in which an electrode has been inserted perpendicular to the cardiac tissue to simulate actual clinical procedures. Temperature-dependent heat capacity, electrical and thermal conductivities, and blood perfusion rate have been considered to model more realistic scenarios. The effects of blood flow and contact force of the electrode tip on the efficacy of a fully coupled model of RFA have been systematically investigated. The numerical study predicts that the efficacy of RFA is significantly dependent on the thermo-electro-mechanical parameters of the cardiac tissue.

Keywords: Radiofrequency Ablation, Cardiac Ablation, Thermo-electro-mechanical Coupling, Contact mechanics, Bio-heat Transfer, Computational Modelling

NOMENCLATURE

c	specific heat capacity (J/(kg·K))
C	tissue water content
E	electric field intensity (V/m)
$\bar{E}$	Young's Modulus of Elasticity (Pa)
F	deformation gradient
$\bar{F}$	exterior body force (N)
h	enthalpy (J/m^3)
H_{fg}	latent heat (J/m^3)
J	volume ratio
k	thermal conductivity (W/m·K)
Q_m	metabolic heat generation (W/m^3)
Q_p	radiofrequency heat source (W/m^3)
t	time (s)
T	temperature (°C)
T_b	core blood (or baseline) temperature
u	mechanical displacement vector (m)
V	electric potential (V)
$\dot{V}$	ablation volume (mm^3)
W	strain energy (J/m^3)
r, z	position/coordinates (m)
α	thermal expansion coefficient (K^{-1})
ε	mechanical strain
ν	Poisson's ratio
ρ	density (kg/m^3)
σ	electrical conductivity (S/m)
$\bar{\sigma}$	mechanical stress (Pa)
δ	Kronecker delta function
ω_b	blood perfusion rate (s^{-1})

Subscripts

b	blood
g	gas phase
l	liquid phase
0	initial value at baseline temperature

[1] Contact author: ssingh@wlu.ca

1. INTRODUCTION

Radiofrequency ablation (RFA) is one of the promising minimally invasive treatment modalities that has been widely and effectively used for treating different types of soft tissue tumors in clinical practices [1]. RFA has also been explored in the treatment of various types of cardiac arrhythmias [2]. During RFA of the cardiac tissue, a radiofrequency (RF) current is delivered into the tissue utilizing the metal electrode that results in the induction of resistive heating at the periphery of the electrode and leads to thermal necrosis or irreversible damage of the cardiac tissue at a temperature greater than 50 °C. The overall goal of the RFA therapy is to maximize the heat transfer within the target tissue that can result in the attainment of the enhanced ablation zone and minimize the effect of factors that hinders the efficient heat delivery to the tissue.

Numerical modeling and simulations play a vital role in the design and development of new systems and protocols for RFA, along with the improvement and optimization of the existing protocols. Numerical simulations serve as a powerful predictive tool for providing *a priori* estimate of the treatment outcomes to the clinical practitioners, rapidly and at a low cost. They also assist in our better understanding of the effects of different extrinsic and intrinsic factors on the efficacy of RFA [3-4]. Several computational studies have been reported in the previous literature on the modelling of cardiac ablation utilizing coupled thermo-electric framework [5-8]. More recently, the mechanical model has also been incorporated in [9,10] for modelling the cardiac tissue deformation under the application of force exerted due to the insertion of the electrode. However, to date, no study has been reported in the previous literature that takes into account the thermo-elastic deformations induced due to the non-uniform temperature distribution within the cardiac tissue during RFA. Importantly, the attainment of higher temperatures within the biological tissues during RFA could significantly contribute to variations in their shape or size due to the induced thermal strain. Thus, in the present study, we report a fully coupled thermo-electro-mechanical model for more accurately quantifying the treatment outcomes of the cardiac ablation. The incorporated mechanical model takes into account the tissue deformation induced due to electrode insertion as well as due to thermal stresses. We investigated the effect of contact force exerted on the cardiac tissue from the electrode and the blood flow rates on the efficacy of cardiac ablation.

2. MATERIALS AND METHODS

Figure 1 presents the two-dimensional axisymmetric computational domain considered in the present study for cardiac ablation, which comprises of a fragment of cardiac tissue, electrode and blood chamber [7]. An open-irrigated electrode (7 Fr diameter and 4 mm length) has been considered that is placed perpendicular to the cardiac tissue and is surrounded by the circulating blood (cardiac chamber) [7,8]. A contact force is applied at the electrode tip of the catheter (i.e. insulated part of the electrode) that results in the mechanical deformation of the tissue surface along with the electrode insertion. Motivated by [8,9], four different values of insertion depth of the electrode have been considered in the present study, viz., 0.5, 1, 1.5 and 2 mm. Notably, considered values of the insertion depth of the electrode lie within the range of contact force between 10 to 40 g that has proved to be safer and effective in clinical trials reported in the previous literature [10]. The thermo-electro-mechanical properties of different materials considered in the present computational study have been summarized in Table 1 [4,7-10].

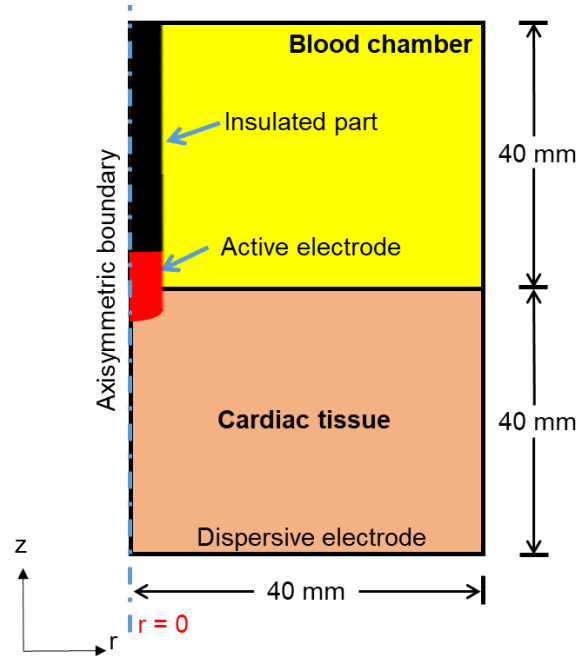

FIGURE 1: SCHEMATIC OF TWO-DIMENSIONAL AXISYMMETRIC MODEL OF THE CARDIAC ABLATION CONSIDERED IN THE PRESENT STUDY (NOT TO SCALE)

TABLE 1: THERMO-ELECTRO-MECHANICAL PROPERTIES OF DIFFERENT MATERIALS CONSIDERED IN THIS STUDY

Parameter	Myocardium/ Cardiac tissue		Blood/ Cardiac chamber	Electrode (Active part)	Catheter (Insulated part)
	Liquid phase	Gas phase			
ρ (kg/m^3)	1060	370.44	1000	21500	70
c (J/(kg·K))	3111	2155.92	4180	132	1045
k (W/(m·K))	$k_0 = 0.54$		0.54	71	0.026
ω_b (s^{-1})	$\omega_{b,0} = 0.017$		–	–	–
σ (S/m)	$\sigma_0 = 0.6$		0.99	4.6×10^6	10^{-5}
α (K^{-1})	1×10^{-4}		–	–	–

2.1 Governing equations for the coupled thermo-electro-mechanical model

The thermal problem of cardiac ablation is solved utilizing the generalized Fourier conduction based Pennes bioheat transfer equation modified by the enthalpy method that incorporates the liquid-vapor phase change to model tissue vaporization within the biological tissue [3,4,8], and is given by:

$$\frac{\partial(\rho h)}{\partial t} = k\nabla^2 T - \rho_b c_b \omega_b (T - T_b) + Q_m + Q_p, \quad (1)$$

where ρ is the density (kg/m^3), h is the enthalpy (J/m^3), ρ_b is the density of blood (kg/m^3), c_b is the specific heat capacity of the blood (J/(kg·K)), k is the thermal conductivity (W/(m·K)), ω_b is the blood perfusion rate (1/s), T_b is the blood temperature (= 37 ^{o}C), T is the unknown temperature to be computed within the cardiac tissue. The term $[\rho_b c_b \omega_b (T - T_b)]$ accounts for the microvascular heat sink effect, Q_p is the radiofrequency heat source (W/m^3) and Q_m is the metabolic heat generation (W/m^3) that has been neglected due to its insignificant contribution in comparison to the other terms [5-10]. Further, the enthalpy of the biological tissue is related to the temperature by:

$$\frac{\partial(\rho h)}{\partial t} = \frac{\partial T}{\partial t} \cdot \begin{Bmatrix} \rho_l c_l & 0 \le T \le 99\ ^0\text{C} \\ H_{fg} C & 99 < T \le 100\ ^0\text{C} \\ \rho_g c_g & T > 100\ ^0\text{C} \end{Bmatrix}, \quad (2)$$

where ρ_i and c_i are the density and specific heat of tissue before phase-change (subscript $i = l$ refers to liquid tissue phase at temperatures below 100 ^{o}C and subscript $i = g$ refers to post-phase-change above 100 ^{o}C), H_{fg} is the latent heat (= 2.162×10^9 J/m^3), i.e., the product of water latent heat of vaporization and water density at 100 ^{o}C, and C is the tissue water content inside the tissue (= 75 %).

Moreover, at the frequency range used during cardiac ablation (≈500 kHz), the wavelength of the electromagnetic field is several orders of magnitude larger than the size of the active electrode and thus, the biological tissue can be considered totally resistive and a simplified version of Maxwell's equations (known as a quasi-static approximation) can be used to solve the electromagnetic problem without compromising accuracy [3]. The volumetric heat generation (Q_p) by electromagnetic field within the biological tissue is given by:

$$Q_p = \sigma |E|^2, \quad (3)$$

where σ is the temperature-dependent electrical conductivity (S/m) and the electric field intensity (E) for the quasi-static approximation of Maxwell's equations is computed from the gradient of voltage (V), as:

$$E = -\nabla V, \quad (4)$$

which in the absence of internal electric sources satisfies the generalized Laplace equation:

$$\nabla \cdot \sigma \nabla V = 0. \quad (5)$$

Further, the electrical conductivity, thermal conductivity and blood perfusion rate of the cardiac tissue have been modelled as a temperature-dependent function [3,8] and are given by Eqs. 6-8, respectively, as:

$$\sigma(T) = \begin{Bmatrix} \sigma_0 \exp^{0.015(T - T_b)} & \text{for } T \le 99\ ^0C \\ 2.5345\sigma_0 & \text{for } 99 < T \le 100\ ^0C \\ 2.534\sigma_0 - 0.502\sigma_0 (T - 100\ ^0C) & \text{for } 100 < T \le 105\ ^0C \\ 0.025345\sigma_0 & \text{for } T > 105\ ^0C \end{Bmatrix}, \quad (6)$$

$$k(T) = \begin{Bmatrix} k_0 + 0.0012(T - T_b) & \text{for } T \le 100\ ^0C \\ k_0 + 0.0012(100\ ^0C - T_b) & \text{for } T > 100\ ^0C \end{Bmatrix}, \quad (7)$$

$$\omega_b(T) = \begin{Bmatrix} \omega_{b,0} & \text{for } T < 50^0 C \\ 0 & \text{for } T \ge 50^0 C \end{Bmatrix}. \quad (8)$$

Motivated by [7,8], the ablation (or damage) volume induced during the cardiac ablation ($\dot{V}$) has been quantified using the 50 ^{o}C isotherm contour (i.e. the volume of cardiac tissue having temperature ≥ 50 ^{o}C post-RFA procedure), which corresponds to a reasonable estimate of the irreversible myocardial injury during hyperthermic ablation, and is given by [11,12]:

$$\dot{V} = \iiint_\Omega dV\ (\text{mm}^3) \quad (\text{where } \Omega \ge 50^0 C). \quad (9)$$

The general form of the thermo-elastic wave equation for the non-rigid mechanics is given by:

$$\rho \frac{\partial^2 u}{\partial t^2} = \bar{\sigma}_{ij,j} + \bar{F}, \quad (10)$$

where ρ is the density, $\bar{\sigma}$ is the stress tensor (i,j = 1,2,3 are the tensor indices representing geometry's coordinate axes), u is mechanical displacement vector, t is time and $\bar{F}$ is the external body force. In the present study, the RF electrode has been modelled as linearly elastic, isotropic and homogeneous material having Young's modulus of elasticity as 168 GPa and Poisson's ratio as 0.38 [10]. The stress-strain relationship for the linearly elastic material is given by:

$$\bar{\sigma}_{ij} = 2\mu\varepsilon_{ij} + \lambda\varepsilon_{kk}\delta_{ij}, \quad (11)$$

where $\varepsilon = [(\nabla u^T + \nabla u)/2]$ is the strain tensor (subscript i ,j = 1, 2, 3 are the tensor indices representing geometry's coordinate axes and subindices $_{kk}$ indicate the trace of the strain tensor), $\mu = [\bar{E}/2(1+\nu)]$ and $\lambda = [\nu\bar{E}/(1+\nu)(1-2\nu)]$ are the Lame's constants$\bar{E}$, is the Young's Modulus of elasticity and ν is the Poissons's ratio and δ is the Kronecker delta function given by:

$$\delta_{ij} = \begin{cases} 1 & for\ i = j \\ 0 & for\ i \ne j \end{cases}. \quad (12)$$

The myocardium tissue has been modelled as a nearly incompressible, isotropic and homogenous hyperelastic material. The Cauchy-stress tensor for the hyperelastic material can be expressed as:

$$\bar{\sigma} = J^{-1} \frac{\partial W(F)}{\partial F} F^T, \quad (13)$$

where F is the deformation gradient and J is the volume ratio (= det(F)) and W is a function of the Green strain components.

In the present study, the Mooney-Rivlin model has been used for describing the strain energy function of the hyperelastic myocardium tissue [10]:

$$W = C_1(I_1 - 3) + C_2(I_2 - 3) + D_1[\exp(D_2(I_1 - 3)) - 1], \quad (14)$$

where I_1 and I_2 are the first and second strain invariants, respectively, C_1 (= 351 Pa), C_2 (= 0), D_1 (= 63.3 Pa) and D_2 (= 5.3) are the material parameters adopted from [10]. Further, the thermal expansion of the hyperelastic myocardial tissue is modelled as:

$$J^{th} = (1 + \varepsilon^{th})^3, \quad (15)$$

where J^{th} is the thermal volume ratio, $\varepsilon^{th}(= \alpha(\mathrm{T} - \mathrm{T}_b))$ is the linear thermal expansion strain and α is the thermal expansion coefficient.

2.2 Numerical setup

A constant power cardiac ablation has been modeled by applying the Dirichlet voltage boundary condition at the active electrode surface whereby a fixed constant voltage of 25 V has been applied for 60 s [6]. The dispersive (ground) electrode has been modelled by applying a 0 V at the bottom surface of the computational domain, so as to mimic the RF current flow between the active and ground electrodes in a monopolar configuration. All the other outer surfaces of the model have been subjected to the Neumann electrical boundary condition of null electric flux. The initial voltage of the entire computational domain has been considered to be 0 V. The effect of the saline flow from the holes of an open-irrigated electrode has been modelled by specifying a constant temperature of 45 °C at the cylindrical zone of the electrode tip, leaving the semispherical part inserted within the tissue free, as in previous numerical studies [7,8]. Notably, this approximation for modelling an open-irrigated electrode has earlier proved to be suitable for predicting the ablation depth and maximum temperature reached within the tissue during cardiac ablation for all time steps [7]. Further, the effect of blood flow inside the cardiac chamber has been modelled by specifying the thermal convective coefficients at the electrode–blood (h_E) and the tissue–blood (h_T) interfaces to reduce computational complexity. Although this modelling approach of blood flow within the cardiac chamber does not provide a realistic blood temperature distribution during cardiac ablation, it does predict the ablation depth reasonably well [7,8]. In the present study, we considered two values of blood velocity, viz., 8.5 cm/s and 3 cm/s representing the high and low blood flow rates within the cardiac chamber, respectively. For these values of the blood flow rates, the respective values of convective heat transfer coefficients are: h_E = 3346 and 2059 W/m^2·K; and h_T = 610 and 265 W/m^2·K corresponding to the high and low blood flow rates, respectively [6,8]. A constant temperature (= 37 °C) thermal boundary condition has been specified at all the outer boundaries of the computational domain that is also the initial model temperature, except at the electrode tip which was considered to be 22 °C, so as to take into account the saline inflow from the open-irrigated electrode [8].

Regarding the mechanical boundary conditions, a prescribed displacement in the vertically downward direction (i.e., - *z*-axis) has been applied to the RF electrode (viz., 0.5, 1, 1.5, 2 mm) to simulate the effect of contact force on the cardiac ablation [9,10]. The prescribed displacement at the electrode surface in the radial direction has been considered to be zero and the fixed constraint on the displacement has been applied at the bottom surface of the computational domain [10]. The initial stress and strain have been set to zero for the entire model. Moreover, the electrical, thermal and mechanical continuity boundary conditions have been imposed at each interface of the computational domain. A finite-element method (FEM) based COMSOL Multiphysics 5.2 software [13] has been used to solve the coupled thermo-electro-mechanical problem using quadratic (second-order) shape functions. It is noteworthy to mention that the computational model of cardiac ablation has been solved in two steps. The first step computes the tissue deformation induced due to the contact force exerted by the RF electrode on the cardiac tissue for different insertion depth of the electrode (= 0.5, 1, 1.5, and 2 mm) considering only the mechanical model, whereby the cardiac tissue is modelled as a hyperelastic material and RF electrode is modelled as a linearly elastic material. In the next step based on the computed deformation of the tissues for different insertion depth of the electrode, a fully coupled thermo-electro-mechanical model has been solved to compute the electric field distributions, temperature distributions, ablation volumes and thermally induced stresses within the cardiac tissue during the RFA procedure. Further, the computational domain has been discretized using the spatial heterogeneous triangular mesh elements. While modelling the first step, where the deformation induced within the cardiac tissue due to the electrode insertion has to be computed, the destination boundary (i.e. cardiac tissue) has finer mesh size compared to the source boundary (i.e. RF electrode). For the second step, where a fully coupled thermo-electro-mechanical model has been solved, an extra mesh refinement has been applied at the electrode-tissue interface where the highest thermal, mechanical and electrical gradients were expected. The final mesh size has been obtained after conducting the mesh convergence tests by progressively refining the mesh until the absolute error for maximum temperature and von Mises stress is less than 0.5 % compared to the previous mesh size and accordingly the previous mesh size was considered as the final optimal mesh size for conducting FEM simulations.

3. RESULTS AND DISCUSSION

The effect of the insertion depth of the RF electrode on the deformation of cardiac tissue during the RFA procedure has been presented in Fig. 2. As mentioned earlier, we have considered four values of the insertion depth, viz., 0.5, 1, 1.5 and 2 mm, in our analysis, so as to mimic the most reliable and frequently utilized range of the penetration depth in clinical trials. As evident from Fig. 2, the deformation of the cardiac tissue at the electrode-tissue interface increases with an increase in the insertion depth of the electrode. The corresponding displacement field distributions have also been presented in Fig. 2 for different

insertion depth of the electrode considered in the present analysis. Further, the comparative analysis of the induced deformation of the cardiac tissue due to RF electrode insertion for different depths has been presented in Fig. 3(a). As evident from Fig. 3(a), the deformation of the cardiac tissue at the electrode-tissue interface is quite predominant for all cases. Moreover, the contact pressure exerted by the electrode on the cardiac tissue has been presented in Fig. 3(b). It can be seen from Fig. 3(b) that the contact pressure increases with the increase in the insertion depth of the electrode and the maximum effect is mainly confined to the radius of the electrode, i.e. up to 1.16 mm. Figure 4 presents the von Mises stress distribution corresponding to different values of the insertion depth of the RF electrode. The maximum value of von Mises stress induced within the cardiac tissue for the electrode insertion depth of 0.5, 1, 1.5 and 2 mm have been found to be 1.61 kPa, 4.50 kPa, 8.03 kPa and 38.8 kPa, respectively. Further, as evident from Fig. 4, the increase in contact force at the electrode results in a significant increase in the induced von Mises stress, which is evident from their wider and deeper reach within the cardiac tissue.

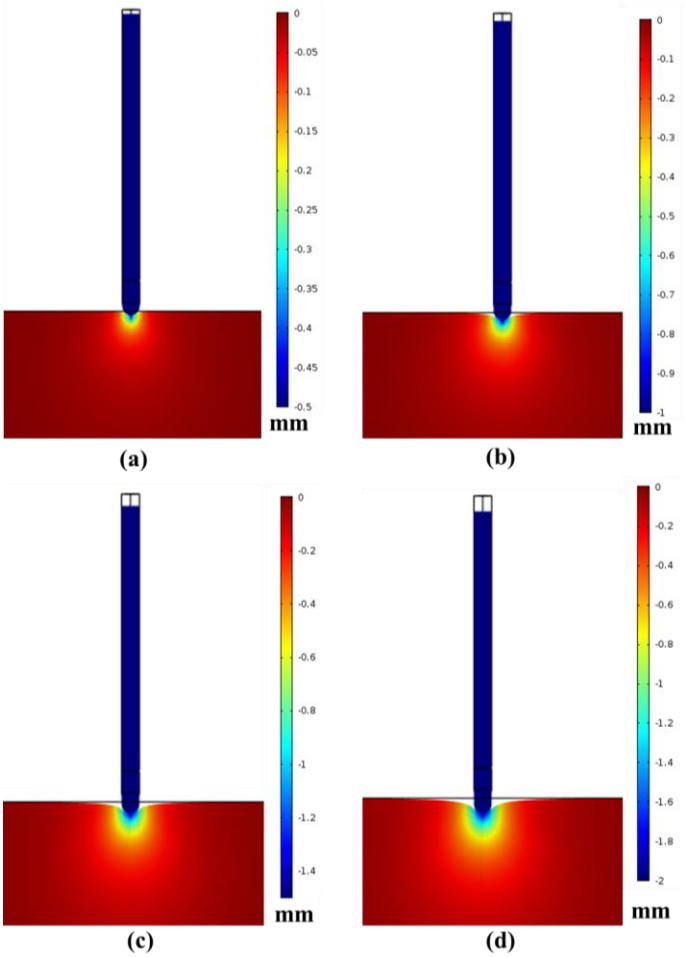

FIGURE 2: (COLOR ONLINE). DISPLACEMENT FIELD DISTRIBUTIONS AND DEFORMATION AT THE ELECTRODE-TISSUE INTERFACE FOR ELECTRODE INSERTION DEPTH OF: (a) 0.5 mm, (b) 1 mm, (c) 1.5 mm AND (d) 2 mm

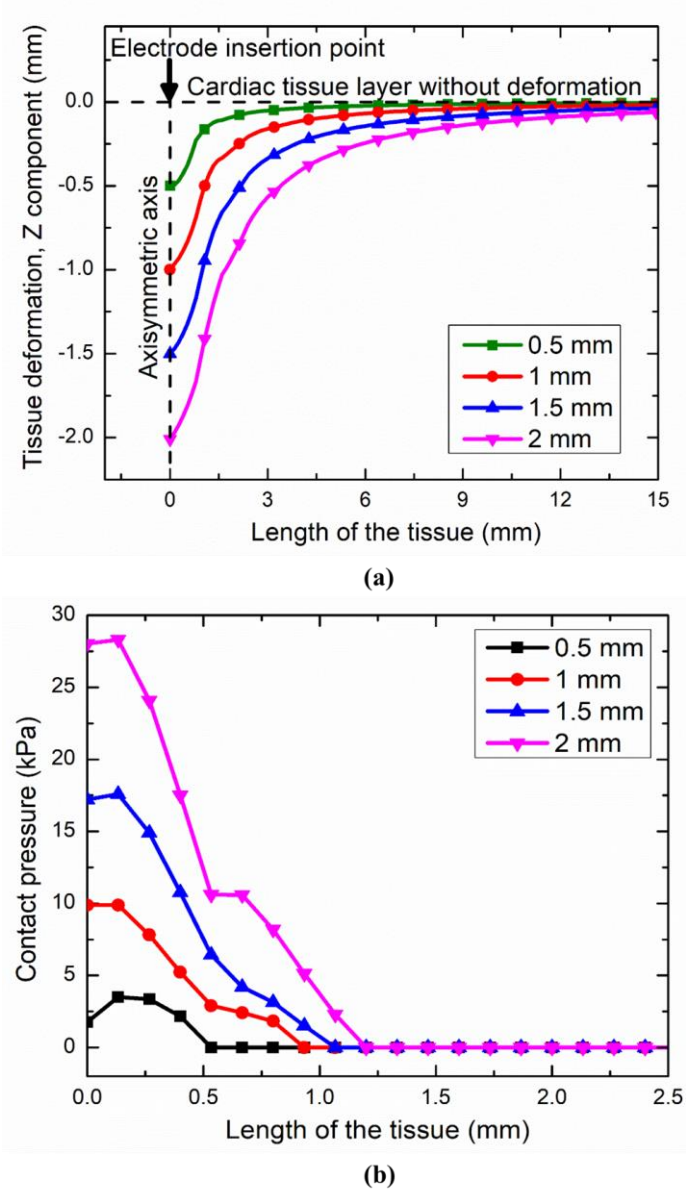

FIGURE 3: (a) TISSUE DEFORMATION AND (b) CONTACT PRESSURE DISTRIBUTION AT THE ELECTRODE-TISSUE INTERFACE FOR THE ELECTRODE INSERTION DEPTH OF: (a) 0.5 mm, (b) 1 mm, (c) 1.5 mm AND (d) 2 mm

The temperature distributions obtained from the fully coupled thermo-electro-mechanical model of cardiac ablation have been presented in Fig. 5 for different values of insertion depth of the electrode, viz., Figs. 5(a)-(b) for 0.5 mm, Figs. 5(c)-(d) for 1 mm, Figs. 5(e)-(f) for 1.5 mm, and Figs. 5(g)-(h) for 2 mm. The left side of Fig. 5 (i.e. Figs. 5(a), (c), (e), (g)) denotes the temperature distribution obtained under the condition of high blood flow rate within the cardiac chamber surrounding the open-irrigated electrode, while the right side (i.e. Figs. 5(b), (d), (f), (h)) denotes the temperature distribution obtained with low blood flow rate condition. It can be seen from Fig. 5 that the blood flow rate within the cardiac chamber significantly affects

the temperature distribution obtained within the cardiac tissue during the RFA procedure and this is true for all values of the RF electrode insertion depths. The maximum values of the temperature within the tissue after 60 s of cardiac ablation for high blood flow conditions have been found to be 84.7 ^{o}C, 89.8 ^{o}C, 94.3 ^{o}C and 94.4 ^{o}C for the electrode insertion depth of 0.5, 1, 1.5 and 2 mm, respectively. While for the low blood flow rate conditions within the cardiac chamber, the maximum values of temperature have been found to be 90.8 ^{o}C, 98.1 ^{o}C, 101.23 ^{o}C and 101.33 ^{o}C for the electrode insertion depth of 0.5, 1, 1.5 and 2 mm, respectively.

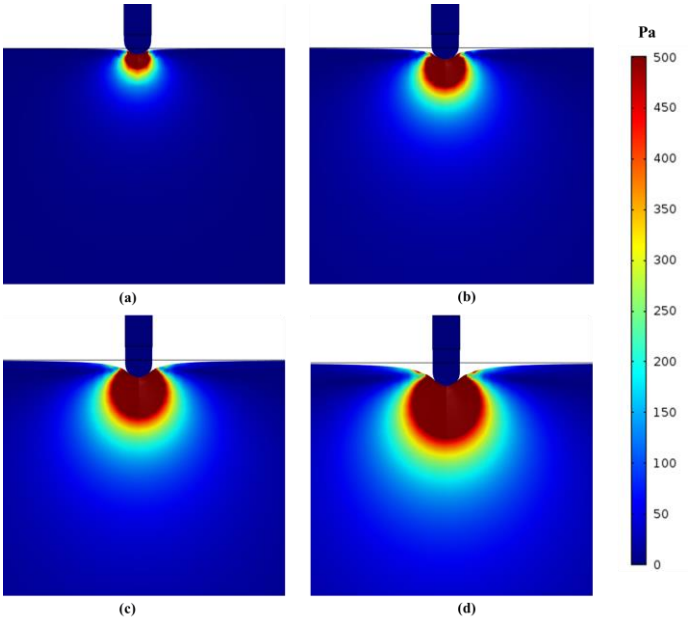

FIGURE 4: (COLOR ONLINE). VON MISES STRESS DISTRIBUTIONS WITHIN THE CARDIAC TISSUE FOR THE ELECTRODE INSERTION DEPTH OF: (a) 0.5 mm, (b) 1 mm, (c) 1.5 mm AND (d) 2 mm

The temporal variation of the ablation volume for different values of the insertion depth of the electrode during the cardiac ablation has been presented in Fig. 6. As evident from Fig. 6, the predicted ablation volume for low blood flow conditions is always higher as compared to the high blood flow condition during the whole ablation time. Moreover, the deviation between the ablation volumes obtained with the high and low blood flow conditions is quite negligible initially up to the first 10 s and increases thereafter. The maximum deviation between the ablation volume obtained with the high and low blood flow conditions has been found for the insertion depth of 0.5 mm. In comparison to the low blood flow, the predicted ablation volumes after 60 s of cardiac ablation with high blood flow decrease by 26.38 %, 25.67 %, 20.23 %, and 18.21 % for the electrode insertion depth of 0.5, 1, 1.5 and 2 mm, respectively. Further, the predicted ablation volumes at the end of 60 s of cardiac ablation procedure increase by 44.76 %, 96.72 % and 117.61 % for the electrode insertion depth of 1, 1.5 and 2 mm, respectively, in comparison to the ablation volume predicted with the electrode insertion depth of 0.5 mm for high blood flow condition. For the low blood flow condition, the respective increase in the ablation volume has been found to be 43.37 %, 81.55 % and 95.87 % for the electrode insertion depth of 1, 1.5 and 2 mm, respectively, when compared to the ablation volume predicted with 0.5 mm electrode insertion depth. This abrupt rise in the predicted ablation volume with the increase of insertion depth of the electrode can be attributed to the fact that the electrode-tissue contact volume increases as the insertion depth or the contact force increases, resulting in improved RF energy delivery to the tissue and thereby enhancing the ablation volume and thus overall efficacy of the cardiac ablation. Conversely, for the low contact force, the majority of the RF energy will be taken away by the blood flow within the cardiac chamber owing to insufficient electrode-tissue contact, and thus reducing the adequate delivery of the energy to the target tissue that further results in decline in the obtained ablation volume.

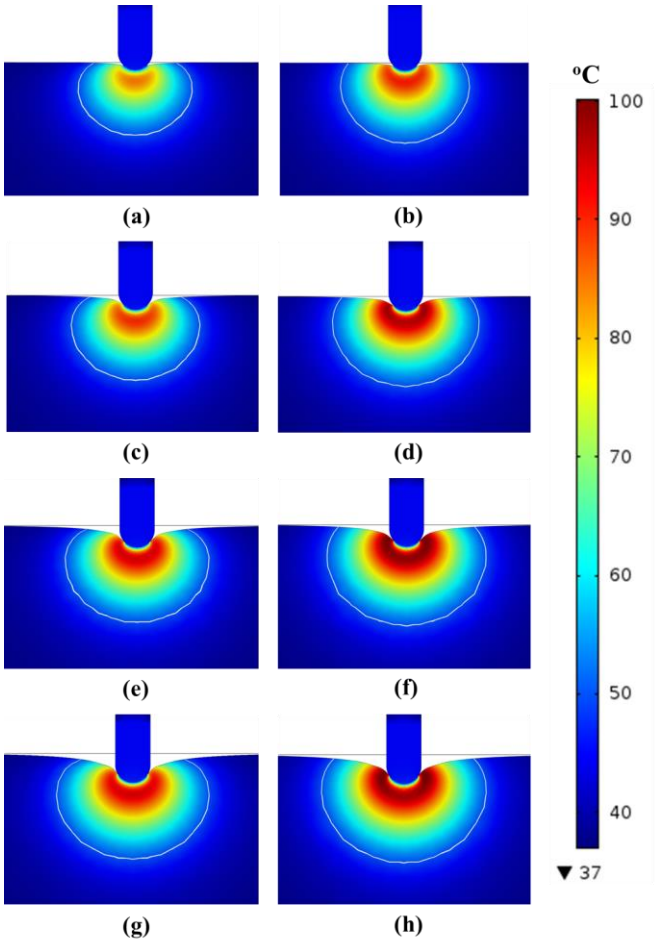

FIGURE 5: (COLOR ONLINE). TEMPERATURE DISTRIBUTIONS OBTAINED IN THE CARDIAC TISSUE AFTER 60 s OF RFA UNDER THE ELECTRODE INSERTION DEPTH OF: (a, b) 0.5 mm, (c, d) 1 mm, (e, f) 1.5 mm AND (g, h) 2 mm. (a, c, e, g) ARE FOR HIGH BLOOD FLOW WHILE (b, d, f, h) ARE UNDER LOW BLOOD FLOW CONDITIONS (SOLID WHITE LINES DENOTES THE LESION BOUNDARIES CORRESPONDING TO 50 ^{o}C ISOTHERM)

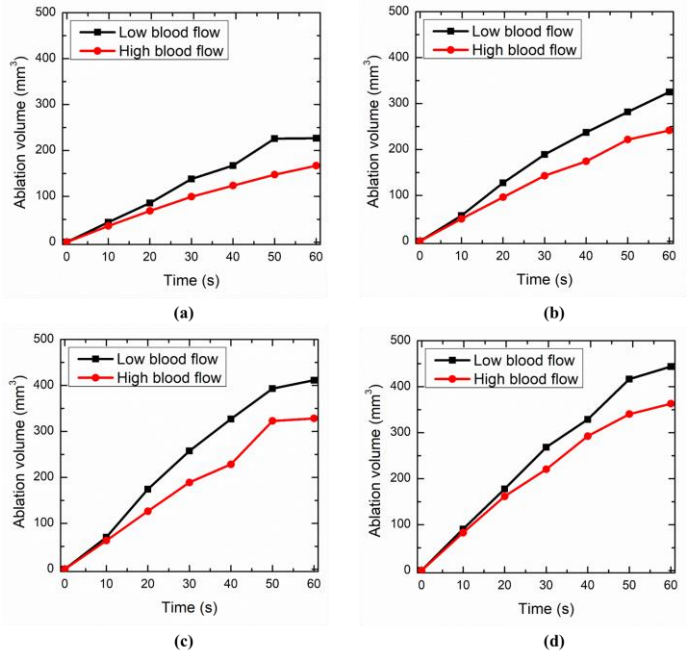

FIGURE 6: TEMPORAL VARIATION OF THE ABLATION VOLUME ATTAINED AFTER 60 s OF CARDIAC ABLATION UNDER THE ELECTRODE INSERTION DEPTH OF: (a) 0.5 mm, (b) 1 mm, (c) 1.5 mm AND (d) 2 mm

The von Mises stresses arising from the thermal exposure of the cardiac tissue to elevated temperature during the RFA procedure has been presented in Fig. 7. It is noteworthy to mention that in continuum mechanics the von Mises stress is the criterion for calculating whether the induced stress will cause the failure of the material or not. As earlier, the left side of Fig. 7 is with high blood flow condition while the right side is with low blood flow condition. Further, Fig. 7(a)-(b) is for 0.5 mm insertion depth, Fig. 7(c)-(d) is for 1 mm insertion depth, Fig. 7(e)-(f) is for 1.5 mm insertion depth, and Fig. 7(g)-(h) is for 2 mm insertion depth. As evident from Fig. 7, the maximum value of the von Mises stress induced within the cardiac tissue has been found to be concentrated close to the vicinity of the electrode tip where the high temperature is found. The maximum value of the von Mises stress induced due to thermal heating of cardiac tissue during RFA lies in the range of 0 to 101 Pa. Further, the induced von Mises stress at the end of 60 s of RFA procedure for low blood flow is slightly higher in comparison to that of high blood flow condition. This can be attributed to the higher value of maximum temperature obtained in the case of low blood flow compared to the high blood flow condition. Thus, the proposed model of cardiac ablation utilizing coupled thermo-electro-mechanical framework would be useful in providing a better and more accurate *a priori* estimates of treatment outcomes to further enhance the efficacy of the procedure. Future studies will be based on developing the fully coupled three-dimensional model whereby the blood flow inside the cardiac chamber and the saline flow through the holes of an open-irrigated electrode will be modelled utilizing the Navier-Stokes equations and the blood will be modelled as a non-Newtonian fluid.

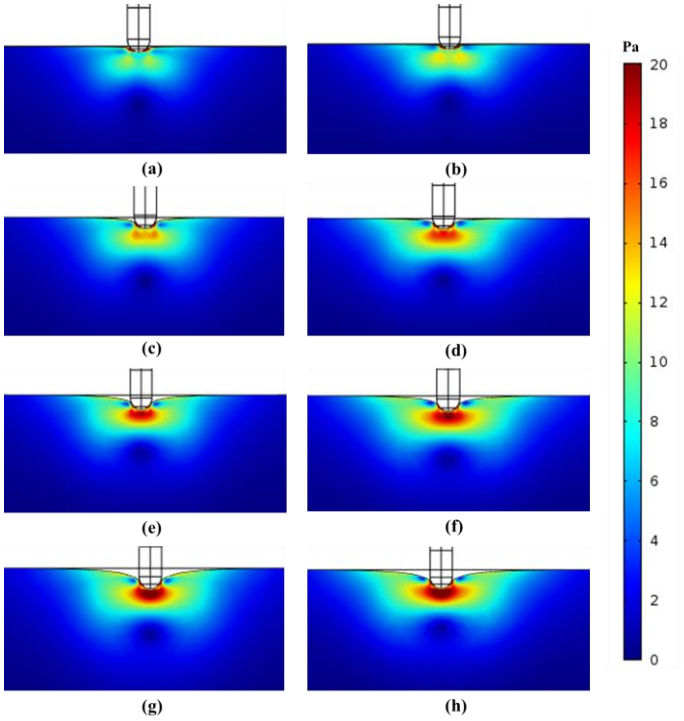

FIGURE 7: (COLOR ONLINE). VON MISES STRESS DISTRIBUTIONS WITHIN THE TISSUE AFTER 60 s OF CARDIAC ABLATION UNDER THE ELECTRODE INSERTION DEPTH OF: (a, b) 0.5 mm, (c, d) 1 mm, (e, f) 1.5 mm AND (g, h) 2 mm. (a, c, e, g) ARE FOR HIGH BLOOD FLOW WHILE (b, d, f, h) ARE UNDER LOW BLOOD FLOW CONDITIONS INSIDE THE CARDIAC CHAMBER

4. CONCLUSION

We have reported a fully coupled thermo-electro-mechanical model of cardiac ablation for a more accurate prediction of the treatment outcomes. Our findings suggest that the ablation volume attained during cardiac ablation is significantly dependent on the contact force at the electrode-tissue interface as well as the blood flow rate. We have also reported the thermal stress distributions induced due to the elevated temperature attained within the cardiac tissue during RFA.

ACKNOWLEDGEMENTS

Authors are grateful to the NSERC and the CRC Program for their support. RM is also acknowledging support of the BERC 2018-2021 program and Spanish Ministry of Science, Innovation and Universities through the Agencia Estatal de Investigacion (AEI) BCAM Severo Ochoa excellence accreditation SEV-2017-0718 and the Basque Government fund AI in BCAM EXP. 2019/00432.

REFERENCES

[1] Singh, Sundeep and Repaka, Ramjee. "Temperature-controlled Radiofrequency Ablation of Different Tissues Using Two-compartment Models." *International Journal of Hyperthermia* Vol. 33 No. 2 (2017): pp. 122-134.

[2] Huang, Shoei K.S. and Wood, Mark A. *Catheter Ablation of Cardiac Arrhythmias*. Elsevier, Philadelphia (2019).

[3] Singh, Sundeep and Melnik, Roderick. "Thermal Ablation of Biological Tissues in Disease Treatment: A Review of Computational Models and Future Directions." *Electromagnetic Biology and Medicine* Vol. 39 No. 2 (2020): 49-88.

[4] Singh, Sundeep and Melnik, Roderick. "Coupled Thermo-electro-mechanical Models for Thermal Ablation of Biological Tissues and Heat Relaxation Time Effects." *Physics in Medicine & Biology* Vol. 64 No. 24 (2019): pp. 245008.

[5] González-Suárez, Ana, Berjano, Enrique, Guerra, Jose M. and Gerardo-Giorda, Luca. "Computational Modeling of Open-Irrigated Electrodes for Radiofrequency Cardiac Ablation Including Blood Motion-Saline Flow Interaction." *PloS ONE* Vol. 11 No. 3 (2016): pp. e0150356.

[6] González-Suárez, Ana and Berjano, Enrique. "Comparative Analysis of Different Methods of Modeling the Thermal Effect of Circulating Blood Flow During RF Cardiac Ablation." *IEEE Transactions on Biomedical Engineering* Vol. 63 No. 2 (2015): pp. 250-259.

[7] Pérez, Juan J., González-Suárez, Ana and Berjano, Enrique. "Numerical Analysis of Thermal Impact of Intramyocardial Capillary Blood Flow During Radiofrequency Cardiac Ablation." *International Journal of Hyperthermia* Vol. 34 No. 3 (2018): pp. 243-249.

[8] González-Suárez, Ana, Pérez, Juan J. and Berjano, Enrique. "Should Fluid Dynamics be Included in Computer Models of RF Cardiac Ablation by Irrigated-Tip Electrodes?." *Biomedical Engineering Online* Vol. 17 No. 1 (2018): pp. 43.

[9] Petras, Argyrios, Leoni, Massimiliano, Guerra, Jose M., Jansson, Johan and Gerardo-Giorda, Luca. "A Computational Model of Open-Irrigated Radiofrequency Catheter Ablation Accounting for Mechanical Properties of the Cardiac Tissue." *International Journal for Numerical Methods in Biomedical Engineering* Vol. 35 No. 11 (2019): pp. e3232.

[10] Yan, Shengjie, Gu, Kaihao, Wu, Xiaomei and Wang, Weiqi. "Computer Simulation Study on the Effect of Electrode–Tissue Contact Force on Thermal Lesion Size in Cardiac Radiofrequency Ablation." *International Journal of Hyperthermia* Vol. 37 No. 1 (2020): pp. 37-48.

[11] Singh, Sundeep, Repaka, Ramjee and Al-Jumaily, Ahmed. "Sensitivity Analysis of Critical Parameters Affecting the Efficacy of Microwave Ablation Using Taguchi Method." *International Journal of RF and Microwave Computer-Aided Engineering* Vol. 29 No. 4 (2019): pp. e21581.

[12] Singh, Sundeep and Melnik, Roderick. "Domain Heterogeneity in Radiofrequency Therapies for Pain Relief: A Computational Study with Coupled Models." *Bioengineering* Vol. 7 No. 2 (2020): pp. 35.

[13] COMSOL Multiphysics® v. 5.2. www.comsol.com. COMSOL AB, Stockholm, Sweden.